

**Department of Physics and Technology
Karazin Kharkiv National University**

**Institut für Kernphysik
Technische Universität Darmstadt**

**Investigation of Dipole and Quadrupole Excitations
Near the Neutron Threshold in the Doubly Magic
Nucleus ^{208}Pb with Resonant Photon Scattering
at the S-DALINAC**

Diploma Thesis

Natalya Ryezayeva

Darmstadt 2001

Abstract

In the following work the investigation of low-lying dipole and electric quadrupole excitations in the doubly magic nucleus ^{208}Pb with the help of real photon scattering is presented. The experimental data making the basis of this work were obtained at the superconducting Darmstadt electron linear accelerator S-DALINAC. A nuclear resonance fluorescence method was used. The energy of electrons and thereby the end-point energy of the continuous bremsstrahlung spectrum of incoming photons was 9 MeV. The photons emitted by the excited nuclei were detected by means of two HPGe detectors.

A detailed picture of the fine structure of the dipole strength near and above the neutron emission threshold in ^{208}Pb has been obtained. About 12 dipole transitions were observed, in particular several transitions were found above the neutron emission threshold. The excitation energies and the ground state transitions widths of the corresponding levels have been determined. The strong fragmentation of the dipole strength was observed. The main E1 strength, observed in this experiment, was concentrated in two energy regions near 5.5 and 7.3 MeV. The last one can be assigned as a possible candidate for Pygmy dipole resonance from comparison with RRPA calculations. The extracted total E1 transition strength in the excitation energy range between 4 MeV and the end-point energy amounted $\sum B(E1)\uparrow = 1191 \cdot 10^{-3} \text{ e}^2\text{fm}^2$. In terms of the energy-weighted electric dipole sum rule, this number corresponds to an exhaustion of 0.98 %, which is in a good agreement with the theoretical predictions.

Of all the observed levels 5 were identified as electric quadrupole, which carry a summed E2 strength of $\sum B(E2)\uparrow = 4940 \text{ e}^2\text{fm}^4$. And 2 transitions were identified as magnetic dipole. One of these M1 transitions was found above the neutron emission threshold and contributes to Giant Magnetic Dipole Resonance, which is concentrated at 7.9 MeV.

Анотація

У даній роботі представлено результати дослідження електричних та магнітних діпольних, а також електричних квадрупольних переходів, що знаходяться в області низьких енергій збудження у двічі магічному ядрі ^{208}Pb , за допомогою резонансного розсіювання реальних фотонів. Експериментальні дані, що полягли в основу цієї роботи, були здобуті на надпровідниковому лінійному прискорювачі електронів S-DALINAC, що розташований у місті Дармштадт (Німеччина). В експерименті була використана метода ядерної резонансної флюоресценції. Енергія електронів, що використовувалися для створення реальних фотонів, дорівнювала 9 МеВ.

Була отримана детальна картина структури діпольної сили навколо та вище за енергію відокремлення нейтронів від ядра ^{208}Pb . Дванадцять діпольних переходів було зареєстровано, декілька з них було знайдено вище порога емісії нейтронів. Були визначені енергії збудження та ширини переходів з відповідних рівней. Спостерігається сильна фрагментація діпольної сили. Головна діпольна електрична сила, що була побачена в цьому експерименті, є зконцентрована у двох областях: навколо 5.5 МеВ та 7.3 МеВ. Засновуючись на порівнянні експериментальних даних із передбаченнями теоретичної моделі випадкових фаз, концентрація сили біля 7.3 МеВ була ідентифікована як можливий кандидат на так-званий "Пігмі" діпольний резонанс. Повна діпольна E1 сила в діапазоні енергій від 4 до 9 МеВ дорвнює в експерименті $\sum B(E1) = 1191 \cdot 10^{-3} \text{ e}^2\text{fm}^2$.

Було ідентифіковано 5 квадрупольних переходів, а також 2 магнітних діпольних переходи, один з яких знаходиться вище порога. Цей рівень дає внесок в гігантський магнітний діпольний резонанс, що зконцентрований навколо 7.9 МеВ.

Contents

| | |
|--|-----------|
| 1 . Introduction | 5 |
| 2 . Nuclear Resonance Fluorescence..... | 7 |
| 2.1 Scattering Cross Sections..... | 7 |
| 2.2 Transition Widths and Reduced Transition Strengths | 11 |
| 2.3 Angular Distributions..... | 11 |
| 3 . Experimental Procedures | 13 |
| 3.1 S-DALINAC and Experimental Facilities..... | 13 |
| 3.2 Experimental Setup | 15 |
| 3.3 The Radiator Target..... | 16 |
| 3.4 The Collimator | 16 |
| 3.5 Detectors | 16 |
| 3.6 BGO Shield..... | 19 |
| 3.7 Experimental Details | 21 |
| 4 . Analysis and Results..... | 23 |
| 4.1 Energy Calibration | 23 |
| 4.2 Assignment of the Transition Multipolarities | 24 |
| 4.3 Further Data Analysis | 25 |
| 4.4 Obtained results | 27 |
| 4.5 Discussion | 34 |
| 5 . Conclusion | 37 |
| 6 . References | 38 |

1. Introduction

Since their discovery giant resonances have attracted much attention because of their fundamental nature [1]. They provide insight into both the effective nucleon-nucleon interaction and other basic properties of nuclei [4]. Strong electric dipole (E1) excitations are usually found at high excitation energies forming a broad structure, which is called giant dipole resonance (GDR). It is well studied [2] since many years and can be understood phenomenologically as a counter-oscillation of protons and neutrons with respect to each other, thus inducing a dynamical electric dipole moment. Due to the repulsive nature of the particle-hole (p-h) interaction, the major part of the total E1 strength is concentrated at high excitation energies of about 10-15 MeV. The systematics of the GDR in heavy nuclei shows, that the centroid excitation energy of such oscillations can be described approximately by the following law:

$$E_x = 79 \cdot A^{-1/3} \text{ [MeV]}, \quad (1.1)$$

where A is a mass number.

In ^{208}Pb it is located around 13.4 MeV and its properties are well known. The experimentally observed dipole strengths of the GDR exhaust almost 100% of the expected total dipole strength, which can be estimated from the Thomas-Reiche-Kuhn energy-weighted sum rule (EWSR), giving the total integrated cross section for electric dipole photon absorption in the absence of exchange forces:

$$\int_0^{\infty} \sigma(E) dE = \frac{2\pi^2 e^2 \hbar}{Mc} \cdot \frac{NZ}{A} = 60 \cdot \frac{NZ}{A} \text{ [mb} \cdot \text{MeV]}. \quad (1.2)$$

Besides the giant dipole mode, one finds E1 transitions also in many nuclei (spherical ones as well as deformed nuclei) at lower excitation energies. Several models predict the existence of such a low-lying electric dipole resonance in stable nuclei with neutron excess [3]. In a classical picture the excess neutrons form a skin around the proton/neutron core with $N \approx Z$ (Fig. 1). A vibration of the skin out of the phase with the stable core can lead to an electric dipole excitation mode.

Since this mode bears resemblance to a "mini" giant dipole resonance it is often called "Pygmy" dipole resonance (PDR) [6,7,8]. The PDR caused by the thin neutron skin in stable nuclei with moderate neutron excess is predicted to be at energies between 6 and 10 MeV with a $B(E1)$ strength in the order of 0,1-1% of the energy-weighted sum rule (EWSR), strongly depending on the N/Z ratio.

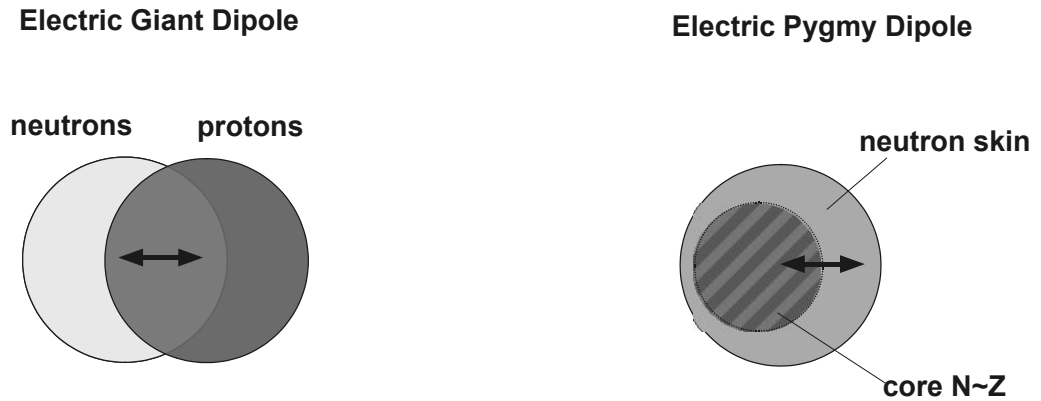


Fig. 1. Macroscopic picture of dipole oscillations in nuclei

For the doubly magic nucleus ^{208}Pb the authors of Ref. [9] predict such a mode to occur at roughly 9 MeV, whereas the hydrodynamic approach of Ref. [10] predicts a soft dipole mode at 4.5 MeV.

The motivation of carrying out the present experiment was mainly the search of a low-lying dipole strength in ^{208}Pb addressing the problem of the Pygmy dipole resonance and two-phonon excitations.

In former years a number of experiments dealing with the investigation of gamma transitions in lead have already been carried out [5,13,14,15]. However, either they had a small end-point energy, not sufficient to cover the whole excitation energy range of interest, or a limited sensitivity to weak transitions needed for such kind of studies. So the aim of this experiment was to study transitions with higher sensitivity and to cover the energy range near and if possible, above the particle emission threshold.

2. Nuclear Resonance Fluorescence

Nuclear Resonance Fluorescence (NRF) represents an ideal tool to investigate low spin states in even-even nuclei excited via dipole and quadrupole transitions from the ground state [16,17]. The specific spin selectivity and low detection limit of this probe allows to study even weak dipole and quadrupole excitations at excitation energies where the level density is already rather high [19].

For NRF experiments one usually uses bremsstrahlung, which can be produced by relativistic electrons. Photons with the resonant energy will excite a target nucleus with a certain probability. This probability can be expressed by the ground state transition width, which is related to the transition strength and to the transition matrix elements. After some fs to ps the excited nuclei will decay either back to the ground state (elastic transition) or to some other low-lying excited state (inelastic transition).

Evaluating the data obtained from an NRF experiment it is possible to determine in a model-independent way a large set of quantities characterising the excited states:

- excitation energies,
- spins and parities (if polarized primary γ -rays are available or a Compton polarimeter is used),
- decay widths,
- lifetimes,
- transition strengths.

2.1 Scattering Cross Sections

Nuclear resonance fluorescence represents the resonant absorption of a real photon by a nucleus, leading to the excitation of a nuclear level and its subsequent decay by reemission of a photon [14].

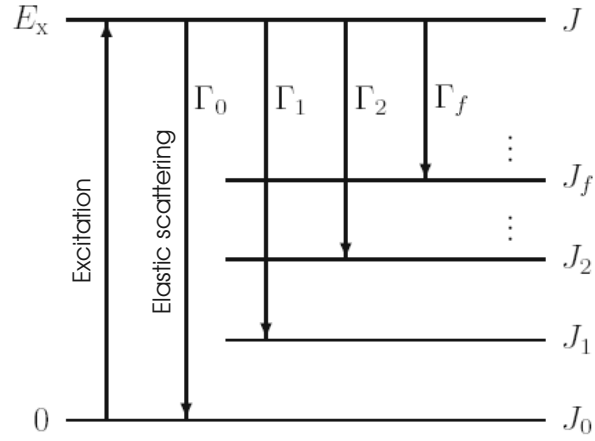


Fig. 2. Gamma transitions in nuclear resonance fluorescence.

The cross section of such a process has a resonance shape and is described by the Breit-Wigner distribution

$$\sigma_{abs}^i(E_\gamma) = \frac{\pi}{2} \cdot g \cdot \frac{\Gamma_0 \Gamma_i}{(E_\gamma - E_x)^2 + \frac{\Gamma^2}{4}}, \quad (2.1)$$

where E_γ is the energy of the incoming photon, Γ is the total decay width of the resonant state at energy E_x , and Γ_i is the partial width for photon decay to the state i ($i = 0$ denotes the ground state), and g is a statistical factor

$$g = \frac{(2J + 1)}{(2J_0 + 1)}, \quad (2.2)$$

with J_0 and J being the spins of the ground and excited state, respectively.

The total decay width Γ is connected to the lifetime τ of the excited level via the uncertainty relation

$$\Gamma = \sum_i \Gamma_i = \frac{\hbar}{\tau}. \quad (2.3)$$

The electromagnetic transitions are characterized by the multipolarity λ with $\lambda = 0, 1, 2, \dots$ for monopole, dipole, quadrupole and other transitions. There exists a selection rule for allowed electromagnetic transitions relating the spins of the initial and final states J_i and J_f with the multipolarity of the transition from these two states:

$$|J_i - J_f| \leq \lambda \leq J_i + J_f. \quad (2.4)$$

The parities of these states define the type of the transition:

$$\pi_i = (-1)^\lambda \cdot \pi_f \quad \text{for electric transitions,} \quad (2.5)$$

$$\pi_i = (-1)^{\lambda+1} \cdot \pi_f \quad \text{for magnetic transitions.} \quad (2.6)$$

The total cross section is given by the sum of partial cross sections of the decays to all possible final states:

$$\sigma_{abs}^{total}(E_\gamma) = \sum_i \sigma_{abs}^i(E_\gamma) = \frac{\pi}{2} \cdot \left(\frac{\hbar c}{E_x} \right)^2 \cdot g \cdot \frac{\Gamma_0 \Gamma}{(E_\gamma - E_x)^2 + \frac{\Gamma^2}{4}} \quad (2.7)$$

If a primary γ -quantum with the energy E_γ is absorbed by a nucleus being initially at rest and in a ground state, then, because of the finite mass of the nucleus, A part of the energy ΔE_{rec} is transferred to the nucleus as a recoil, so that $E_\gamma = E_x + \Delta E_{rec}$, with

$$\Delta E_{rec} = \frac{E_\gamma^2}{2Mc^2}, \quad (2.8)$$

where M is the rest mass of the emitting nucleus. The excited nucleus is not at rest any more, but is moving in the direction of the primary photon beam. If during the short (from fs to ps) decay time to the ground state a secondary γ -quantum is emitted, its energy will experience a Doppler shift in addition to the recoil correction. Thus, the emitted photon will have a different energy dependence on the emission angle Θ with respect to the direction of the primary photon, which excited the nucleus:

$$E_{\gamma'} = E_\gamma - \frac{E_\gamma^2}{2Mc^2} \cdot [1 - 2\cos\Theta] \quad (2.9)$$

If this energy difference is large compared to the width of the level, as is generally the case, then the cross section for resonance absorption of the emitted photon by some another neighbouring nucleus becomes extremely small. This is a precondition to make the detection of emitted photons with the NRF method possible at all.

Another factor of great importance for NRF experiments is the thermal motion of the atoms in the target. This motion causes a Doppler broadening of the absorption line width, which is generally several orders of magnitude larger than the natural width of the emission and absorption lines. It can be assumed that the thermal velocities of nuclei v have a Maxwell distribution [18]

$$f(v) = \left(\frac{M}{2\pi kT} \right)^{\frac{1}{2}} \exp\left(- \frac{Mv^2}{2kT} \right), \quad (2.10)$$

where M is the nuclear mass, k is the Boltzmann constant, and T the absolute temperature. Then instead of Eq. 2.1 we obtain the Doppler-broadened Breit-Wigner distribution

$$\sigma_{DBW}^i(E_\gamma, T) = 2\pi \cdot \left(\frac{\hbar c}{E_x} \right)^2 \cdot g \cdot \frac{\Gamma_0}{\Gamma} \cdot \frac{\Gamma_i \sqrt{\pi}}{2\Delta} \exp\left(- \frac{E_\gamma - E_x}{\Delta} \right)^2, \quad (2.11)$$

where Δ is a Doppler width

$$\Delta = \left(\frac{E_\gamma}{c} \right) \cdot \left(\frac{2kT}{M} \right)^{\frac{1}{2}}. \quad (2.12)$$

Since the energy resolution of HPGe detectors widely used for the detection of the emitted photons is usually worse than the Doppler broadening of line widths, one practically measures the integrated cross section I_i which can be deduced by integration of Eq. 2.11 over the entire range of photon energies

$$\begin{aligned} I_i &= \int \sigma_{DBW}^i(E_\gamma, T) dE_\gamma \\ &= \pi^2 \cdot \left(\frac{\hbar c}{E_x} \right)^2 \cdot g \cdot \frac{\Gamma_0 \Gamma_i}{\Gamma}. \end{aligned} \quad (2.13)$$

In the case of the elastic transitions ($\Gamma_i = \Gamma_0$) we have

$$I_0 = \pi^2 \cdot \left(\frac{\hbar c}{E_x} \right)^2 \cdot g \cdot \frac{\Gamma_0^2}{\Gamma}. \quad (2.14)$$

2.2 Transition Widths and Reduced Transition Strengths

The ground state decay width Γ_0 is proportional to the reduced transition probability $B(\Pi\lambda, E_\gamma)^\uparrow$:

$$\Gamma_0 = 8\pi \sum_{\Pi\lambda=1}^{\infty} \frac{(\lambda + 1) \cdot (E_\gamma/\hbar c)^{2\lambda+1}}{\lambda[(2\lambda + 1)!]^2} \cdot \frac{2J_0 + 1}{2J + 1} \cdot B(\Pi\lambda, E_\gamma)^\uparrow, \quad (2.15)$$

where $\Pi=E$ for electric transitions and $\Pi=M$ for magnetic transitions. The photon can transfer only a small momentum to a nucleus. Therefore in NRF experiments one excites mostly dipole transitions and to a lesser extent quadrupole transitions.

For even-even nuclei one has the following relation between reduced transition strength and the ground state decay width

$$\frac{B(E1)^\uparrow}{[e^2 fm^2]} = 9.554 \cdot 10^{-4} \cdot g \cdot \frac{\Gamma_0}{[meV]} \cdot \left(\frac{[MeV]}{E_x} \right)^3, \quad (2.16)$$

$$\frac{B(M1)^\uparrow}{[\mu_N^2]} = 8.641 \cdot 10^{-2} \cdot g \cdot \frac{\Gamma_0}{[meV]} \cdot \left(\frac{[MeV]}{E_x} \right)^3, \quad (2.17)$$

$$\frac{B(E2)^\uparrow}{[e^2 fm^4]} = 1.245 \cdot 10^3 \cdot g \cdot \frac{\Gamma_0}{[meV]} \cdot \left(\frac{[MeV]}{E_x} \right)^5. \quad (2.18)$$

The reduced transition probabilities $B(\Pi\lambda; J \rightarrow J_0) = B(\Pi\lambda)^\downarrow$ and $B(\Pi\lambda; J_0 \rightarrow J) = B(\Pi\lambda)^\uparrow$ differ by the statistical factor introduced in Eq. 2.2

$$B(\Pi\lambda)^\uparrow = \frac{2J+1}{2J_0+1} \cdot B(\Pi\lambda)^\downarrow. \quad (2.19)$$

2.3 Angular Distributions

The multipole order (dipole or quadrupole) of a transition can be determined in NRF experiments by measuring angular distributions of emitted photons with respect to the incoming photon beam [19]. The angular correlation

function $W(\Theta)$ of the scattered photon can be written as a sum of even Legendre polynomials $P_\nu(\Theta)$:

$$W(\Theta) = \sum_{\nu=0,2,4,\dots} A_\nu^{i \rightarrow j} \cdot A_\nu^{j \rightarrow k} \cdot P_\nu(\cos \Theta) , \quad (2.20)$$

where Θ is the angle between scattered and primary photon.

Angular distributions of photons scattered off an even-even nucleus through pure dipole (spin sequence 0-1-0) and quadrupole (spin sequence 0-2-0) transitions are given by

$$W(\Theta)_{Dipole} = \frac{3}{4} \cdot (1 + \cos^2 \Theta) , \quad (2.21)$$

$$W(\Theta)_{Quadrupole} = \frac{5}{4} \cdot (1 - 3 \cos^2 \Theta + 4 \cos^4 \Theta) . \quad (2.22)$$

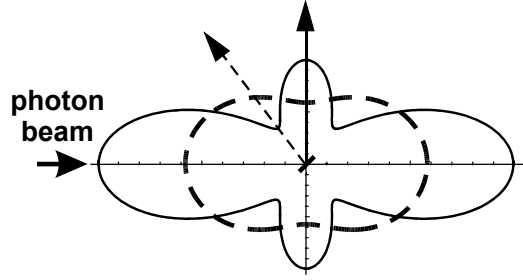


Fig. 3. Angular correlations for dipole (0-1-0, dashed curve) and quadrupole (0-2-0, solid curve) transitions.

As can be seen from Fig. 3, at 90° the angular distribution for dipole transitions has a minimum, whereas for quadrupole transitions it has a maximum at 90° and two minima at 53° and 127° . Therefore placing detectors at these angles and comparing the intensities of lines one can distinguish between quadrupole and dipole transitions.

The angles $\Theta = 127^\circ$ is more favourable than $\Theta = 53^\circ$ because of the dramatic background decrease at backward angles. The intensity ratio $W(90^\circ)/W(127^\circ)$ is 0.73 and 2.28 for dipole and quadrupole transitions, respectively. The difference between these theoretical values is slightly reduced for the realistic geometries used because of the finite opening angles of the detectors in the (γ, γ') experiments.

3. Experimental Procedures

3.1 S-DALINAC and Experimental Facilities

The photon scattering experiment was performed at the superconducting Darmstadt electron linear accelerator S-DALINAC [20]. This accelerator has been constructed under the leadership of Professor Dr. Dr. h.c. mult. Achim Richter at the Institute for Nuclear Physics of the Darmstadt University of Technology. It became the first superconducting continuous-wave linear accelerator of electrons in Europe. Since 1991 S-DALINAC delivers electron beam with the maximum energy of 130 MeV and the current of 40 μA for a wide range of nuclear physics experiments. The layout of the accelerator S-DALINAC is shown in Fig. 4.

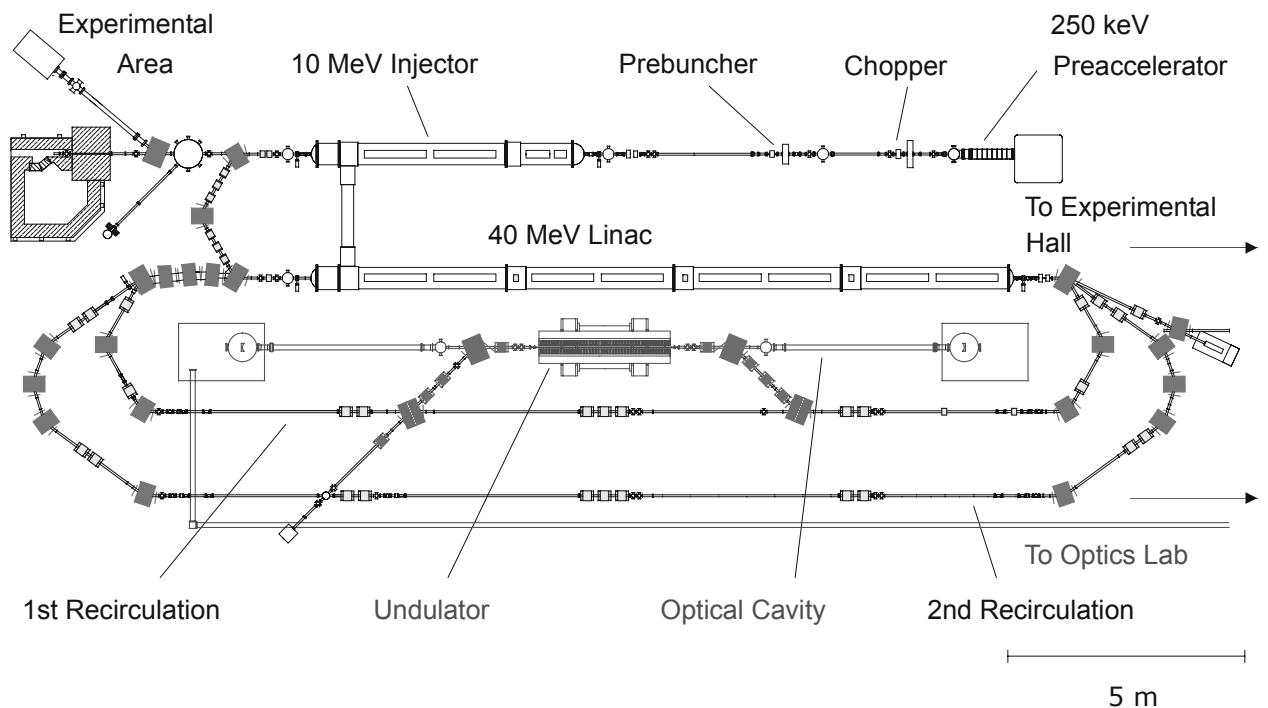


Fig. 4. Schematic layout of the S-DALINAC.

The electrons are emitted by a cathode and then accelerated electrostatically to an energy of 250 keV. The required time structure of the electron beam for radio-frequency acceleration in a 3 GHz field is prepared by a chopper/prebuncher system operating at room temperature. The superconducting injector linac consists of one 2-cell, one 5-cell, and two standard 20-cell Niobium structures, cooled to a temperature of 2 K by liquid helium. When leaving the

injector, the beam has an energy up to 10 MeV and can either be used for radiation physics experiments or for nuclear resonance fluorescence experiments. Alternatively it can be bent by 180° , and injected into the main accelerator section. This superconducting linac has eight 20-cell cavities which provide an energy gain of up to 40 MeV. After passing through the main linac the electron beam may be extracted towards the experimental hall or it can be reinjected twice into the main linac using two separated recirculating beam transport systems. After three passes the electron beam with an energy of up to 130 MeV is delivered to several experimental facilities, schematically shown on the Fig. 5. A wide range of electron scattering experiments is carried out using a large spatial and momentum acceptance magnetic spectrometer of QCLAM type or another magnetic spectrometer of energy-loss type. Additionally, in the first recirculation beam-line a Free Electron Laser (FEL) is located.

S-DALINAC

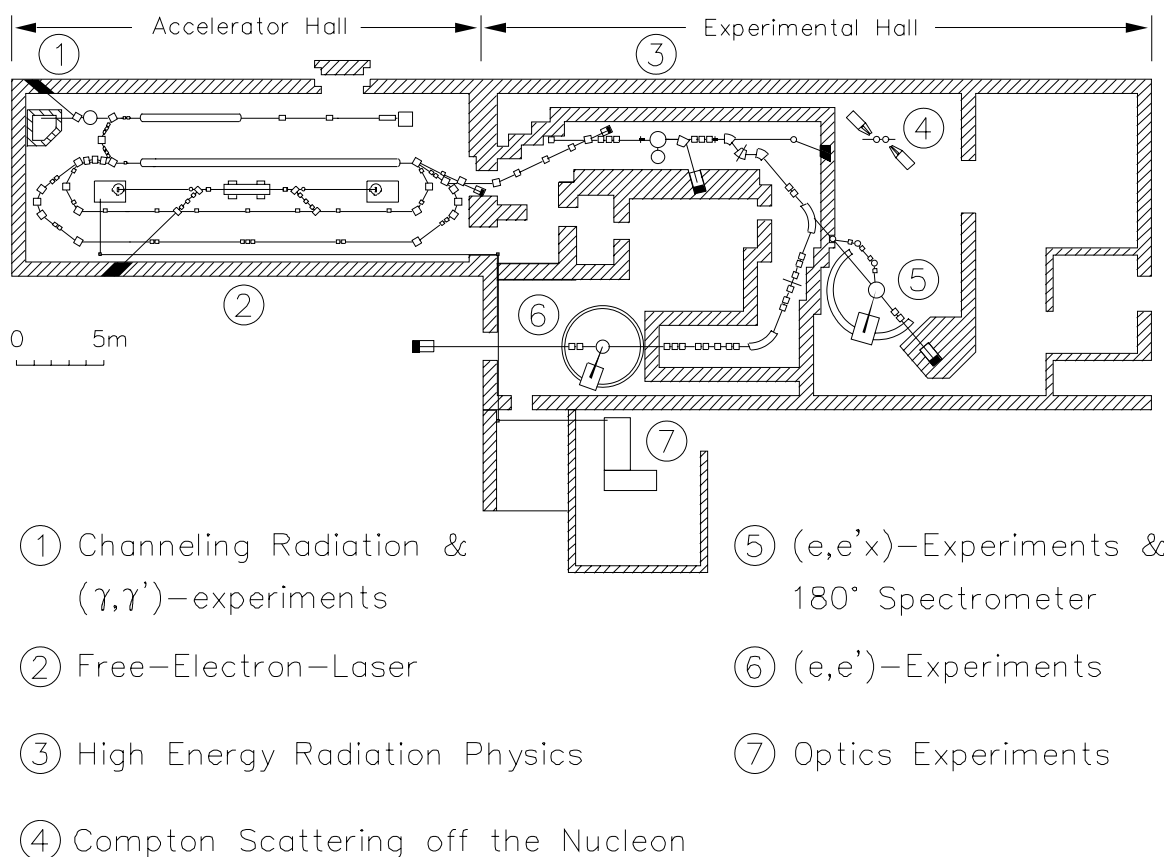


Fig. 5. Experimental facilities at the S-DALINAC.

3.2 Experimental Setup

In NRF experiments the targets of interest are irradiated by a continuous bremsstrahlung beam, which is produced by decelerating electrons in a massive conversion target, called radiator. The photon beam cone is defined geometrically by means of a collimator behind the radiator. The NRF facility at the S-DALINAC [21], shown in Fig. 6, uses the 10 MeV injector of the S-DALINAC which delivers a continuous-wave electron beam with currents up to $60 \mu\text{A}$. In the present setup a relatively close geometry between radiator, target, and detectors has been chosen to obtain a higher photon flux. The distance between the radiator and the target for the photon scattering experiments (NRF target) is about 1.5 m. The photon flux is monitored by an ionization chamber located about 1 m behind the NRF target. Scattered photons are detected by high purity Germanium Crystal detectors (HPGe) having an efficiency of photon detection of 100% relative to a $3'' \times 3''$ standard NaI detector. The detectors were positioned at 90° and 130° with respect to the direction of the incoming photon flux.

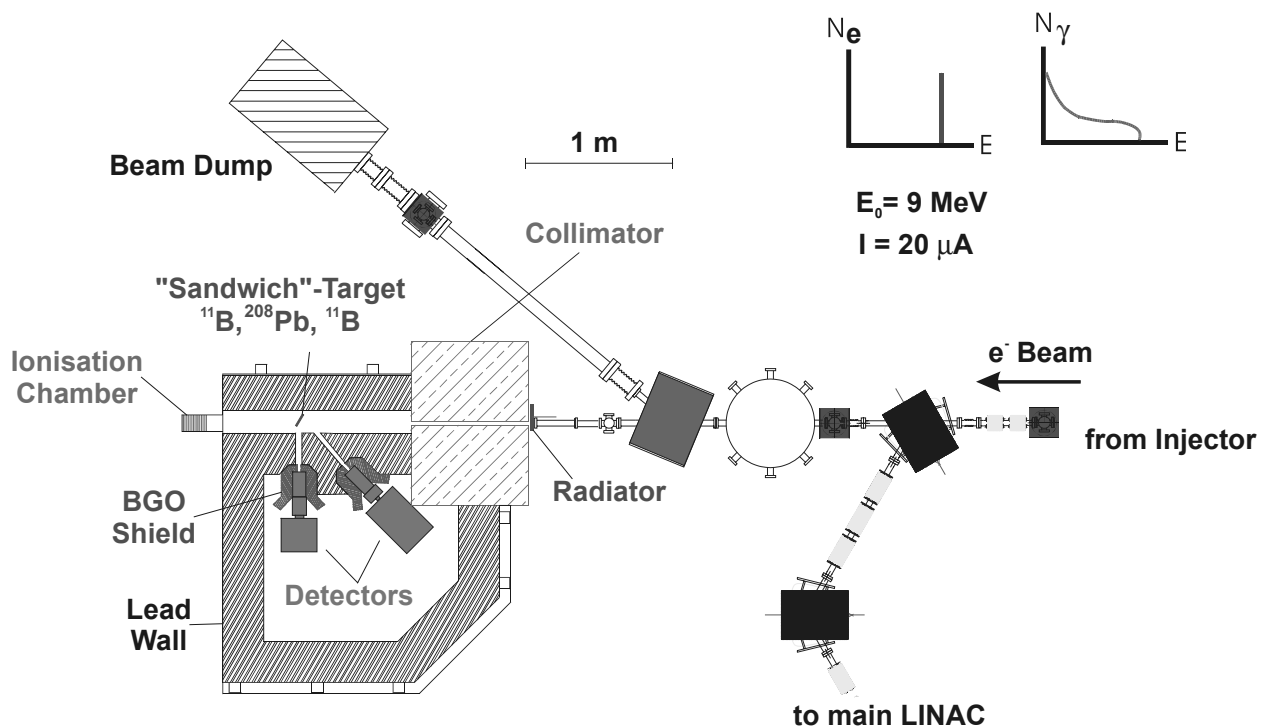


Fig. 6. Schematic layout of the NRF setup at the S-DALINAC

3.3 The Radiator Target

The facility for NRF experiments uses a 14 mm thick copper radiator to produce neutron-free continuous γ -spectra with energies up to 10 MeV. The additional requirements on any material for a radiator are a high heat conductivity and a high melting point to avoid the melting of the radiator. The radiator was additionally cooled by the air fan.

3.4 The Collimator

The maximum energy of the photons, which can be achieved by the injector at the S-DALINAC is about 10 MeV. Therefore to decrease the background from the neutrons produced in (γ, n) reactions one has to use a material for the photon collimator and radiator having neutron separation energies around 10 MeV for all stable isotopes. The neutron separation energies of the copper isotopes match exactly the conditions at the injector of the S-DALINAC.

The collimator hole has a conical shape, changing from a diameter of 12 mm at the entrance to 20 mm at the exit. Additional copper bricks were arranged around the collimator on the radiator side. Because the bremsstrahlung is emitted mainly in forward direction, this setup avoids neutron-induced background from the collimator. The remaining area between the radiator and the detectors is filled with iron and lead to reduce the γ -ray flux at the detector positions.

3.5 Detectors

The detectors used in the present experiment were of HPGe type. The high purity germanium (HPGe) detector is a semiconductor detector based on a reverse biased p-n junction [22,23]. It has a density of impurities of less than 10^{10} atoms/cm³, compared with 10^{12} atoms/cm³ for normal semiconductors.

The HPGe crystal purity is not affected by temperature, allowing storage without cooling, but due to the small band gap of germanium (0.7 eV), they must be cooled to liquid nitrogen temperature 77K in order to reduce thermal noise during operation. For gamma-ray spectroscopy, an active volume as large as

possible is required, so detectors are constructed in a bulletized coaxial shape (Fig. 7).

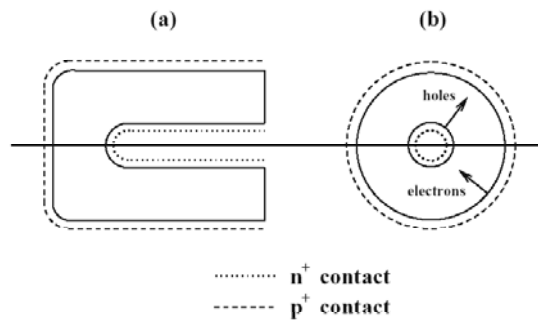


Fig. 7. Bulletized n-type coaxial HPGe detector: (a) is a view perpendicular to and (b) is through the axis of the crystal. The electrical contact surfaces are shown.

A part of the central core is removed and the electrical contacts are attached at the centre and the outside of the crystal. In an n-type detector the inner contact is a thick n⁺ contact ~600 μm thick and the outer contact a thin p⁺ contact 0.3mm thick (the + sign convention usually refers to a highly doped material). This is a usual arrangement for gamma-ray spectroscopy since the thick n⁺ contact would produce greater attenuation at the outside edge.

The photon coming into such a detector, loses its energy in the Ge-crystal, producing particle-hole pairs in the semiconductor. This is realized via the processes of Compton-effect, photoeffect, and pair production. The charge produced is proportional to the energy deposited by the photon in the crystal. The energy required to form an electron-hole pair in HPGe detectors is about 3 eV. This means that a large number of electron-hole pairs can be formed, and so many charge carriers are released for each gamma-ray interaction. This has two consequences: first, there is a small statistical fluctuation in the number of charge carriers per pulse, and second, as a result of the large number there is an excellent signal to noise ratio, both leading to a good energy resolution.

A schematic construction of a typical HPGe detector is shown in Fig. 8.

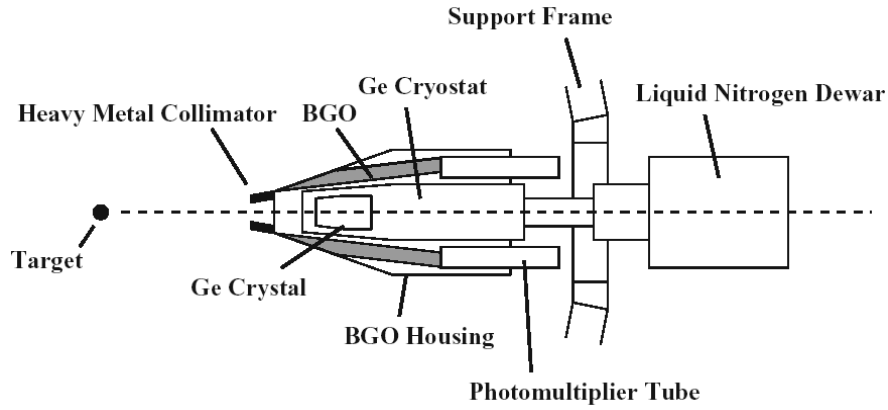


Fig. 8. Construction of a typical HPGe detector with BGO shield.

For the detection of the emitted gamma radiation two HPGe detectors were used in the present experiment. The first detector was positioned at 90° with respect to the primary beam axis. Further on it will be called “Compton-Polarimeter”, or simply “Polarimeter” [24]. It consisted from a large Germanium-crystal cylinder with a volume of 362 cm^3 .

The outer contact of the Polarimeter crystal is divided into four equal parts, allowing to readout the signal from each of the four segments of a crystal separately. At the same time one can read out the signal via the inner contact giving the full energy lost by the photon in the detector. The information from the separate sections can be used for the determination of the parity of the transition. This is based on the measurement of the polarization of the emitted photon using the feature that the direction of emission of Compton-scattered photon depends on the polarization of the incoming photon. At 90° relative to the incoming photon beam the electric field vectors of E1 radiation are perpendicular to the reaction plane whereas for E2 and M1 photons they are orientated parallel to the reaction plane. The photon which experiences Compton scattering near the border between two sections of the crystal, can then be detected also in the neighbouring section. So, one sets the coincidence logic between signals from the neighbouring segments, so that one can detect horizontally and vertically Compton-scattered photons. Provided that the multipolarity of the transition is known, one thus obtains the parity of the excited level [25,26]. However, good statistics is crucial in such studies. In the present experiment it was possible in principle to conduct such

analysis for the strongest transitions, but it was not necessary as the parities of the strong transitions in ^{208}Pb are already known.

The second detector, called “Detector”, was positioned at the angle of 130° . Its crystal had a volume of 375.7 cm^3 . Both detectors had an efficiency of about 100% relative to the 3" x 3" NaI crystal.

The detectors were surrounded by massive lead walls (more than 10 cm thick) in order to shield them against gamma-radiation coming from the accelerator. Only from the target side openings with a diameter of 5 cm existed. In front of each detector thin copper bricks were placed to suppress low-energy gammas coming from the target.

3.6 BGO Shield

For the detection of the photon it is desirable that the photon loses all its energy in the crystal. Those events, in which only a part of the photon energy is deposited in the crystal, should be regarded as incomplete, because they can not be used for the analysis of the present experiment. In order to suppress such events a so-called BGO shield was used [27]. It is a detector based on an inorganic bismuth germanate scintillator ($\text{Bi}_4\text{Ge}_3\text{O}_{12}$). The large atomic number of Bi ($Z=83$) and its high density (7.3 g/cm^3) make BGO ideal for the detection of γ rays. In comparison with NaI, another commonly used scintillator, 6 cm of BGO-shield is required to absorb a 1 MeV γ ray, whereas 14 cm would be required for NaI. Thus only a small amount of BGO is required to absorb γ rays. However, BGO has a lower light yield ($\approx 15\%$). Therefore BGO is used when the need for high γ -ray counting efficiency outweighs the need for energy resolution. This scintillator has a much lower energy resolution in comparison with the HPGe-detector, but the detection efficiency is also 100% relative to the NaI crystal. An electrical anticoincidence between the signals from the main HPGe crystal and the BGO-shield was set up. All those events in which a signal was simultaneously registered

by the detector and by the BGO shield were treated as a background and were ignored.

Besides Compton-scattered γ -quanta also events from cosmic rays can contribute to the background in the spectrum. These events can also be suppressed by the BGO shield. Moreover by use of a BGO one can significantly reduce single-escape (SE) and double-escape (DE) lines. These are the peaks at energies of 511 keV and 1022 keV below the photopeak energy respectively. At energies larger than twice the rest mass of the electron pair production is possible. The positron may then annihilate with an electron and emit two 511 keV γ rays which may be detected in the annihilation peak. This process is displayed in Fig. 9.

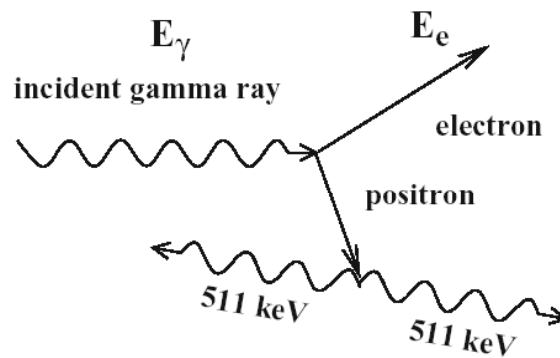


Fig. 9. Positron annihilation and the origin of single- and double-escape peaks.

It may happen, however, that one or both photons escape the detector without further interaction. Then SE and DE will be observed at energies of $E_\gamma - 511$ keV and $E_\gamma - 1022$ keV. The advantage of such an active shielding especially for high γ -energies up to 10 MeV is demonstrated in Fig. 10. One can see a significant reduction of the background. Besides SE, the BGO shield could fully suppress DE peaks.

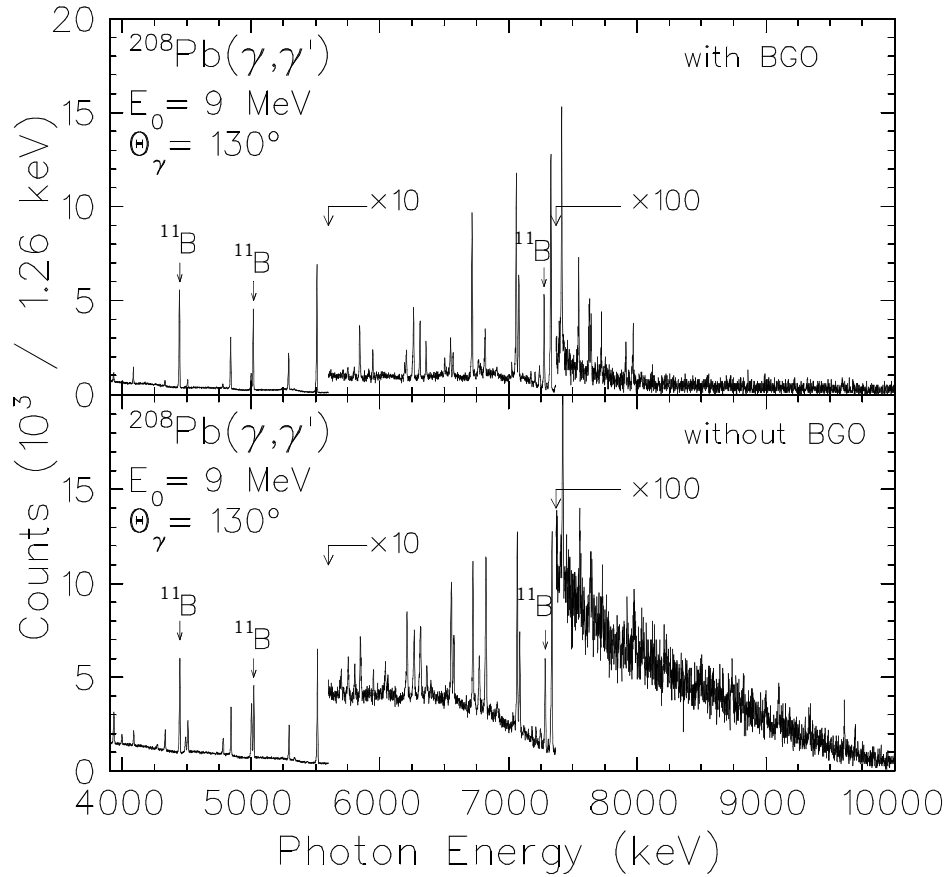


Fig. 10. Spectrum detected at 130° with and without BGO shield.

3.7 Experimental Details

The experiment was carried out in spring 2001. Electrons with an energy of 9 MeV were used to generate bremsstrahlung spectra.

A target made of highly-enriched ^{208}Pb (>99%) material having a weight of 1205 mg was pressed into a pill with the diameter of 20 mm and was sandwiched between two thin layers of $^{\text{nat}}\text{B}$ with weight 1543.5 mg. The well-known transitions in ^{11}B , which has an abundance of 80.1% of $^{\text{nat}}\text{B}$, were used for energy calibration of the detectors and also for the photon flux and efficiency determination. In addition, placing Boron targets on the front and the back side of the ^{208}Pb target allowed to correct for the effect of photon flux decrease in the target.

The γ -decay of the excited levels was observed with the two HPGe detectors described above, which were positioned at 90° and 130° with respect to

the incoming photon beam at distances of 26 cm and 26.5 cm from the target, respectively.

Both detectors were surrounded by active BGO shield. Counting rates were 6000 kHz in the Polarimeter and 7000 kHz in the Detector. Application of BGO anticoincidence condition resulted in a decrease of the counting rates to 3000 kHz and 2400 kHz. The dead-time of the Polarimeter and the Detector were correspondingly 4.7% and 3.1% respectively.

Behind the target an ionisation chamber was used for monitoring the photon flux. The beam transport system was optimized to achieve the maximum current in the ionisation chamber which corresponded to the maximum of the photon flux on the target.

During the experiment the energy of the electrons and the electron beam quality were periodically controlled by deflecting the electron beam at 40° by means of a dipole magnet and by checking the position and the spatial distribution of the beam spot on a scintillating target with a video camera.

The average electron beam current was 20 μA . The total time of the measurement was about 50 hours.

4. Analysis and Results

4.1 Energy Calibration

The γ -quanta being stopped in the crystal lead to the creation of a certain amount of free charge, which by means of the detector electronics is collected, amplified and converted into a voltage. The output voltage is proportional to the energy lost by the γ -quantum. It is digitized by means of an analog-to-digital converter and transferred to a PC. Raw spectra for both detectors are created, each raw spectrum having 8192 channels. In order to find the correspondence between the channels and the energy a calibration target is used, for which the energies of γ -lines are well known. Here ^{11}B was used. In the calibration procedure the recoil and Doppler corrections of the boron lines were taken into account. The result of such a calibration is shown in Fig. 11.

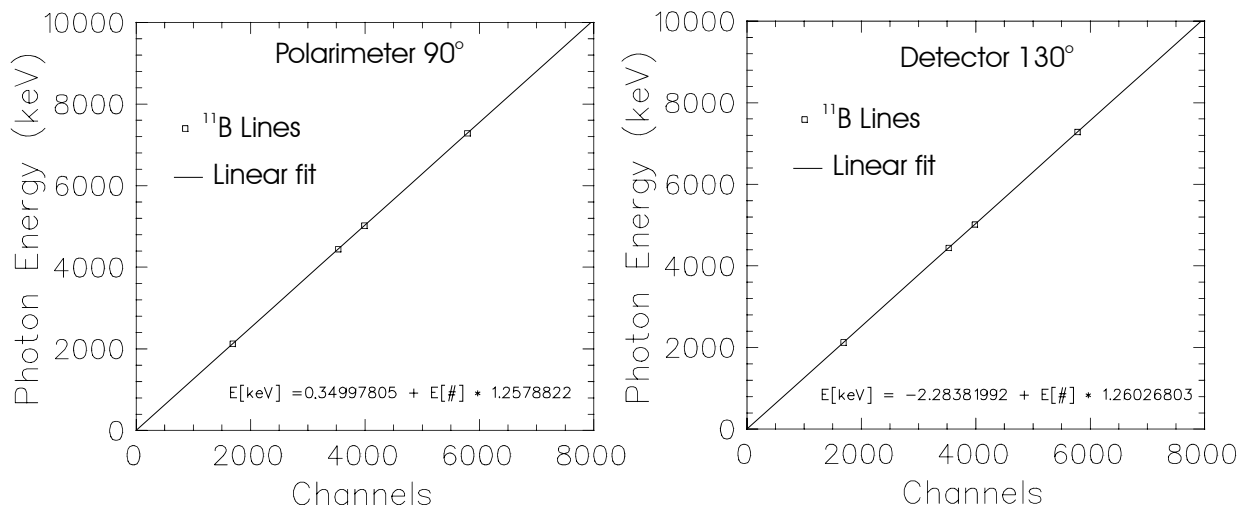


Fig. 11. Energy calibration of the detectors using known transitions in ^{11}B .

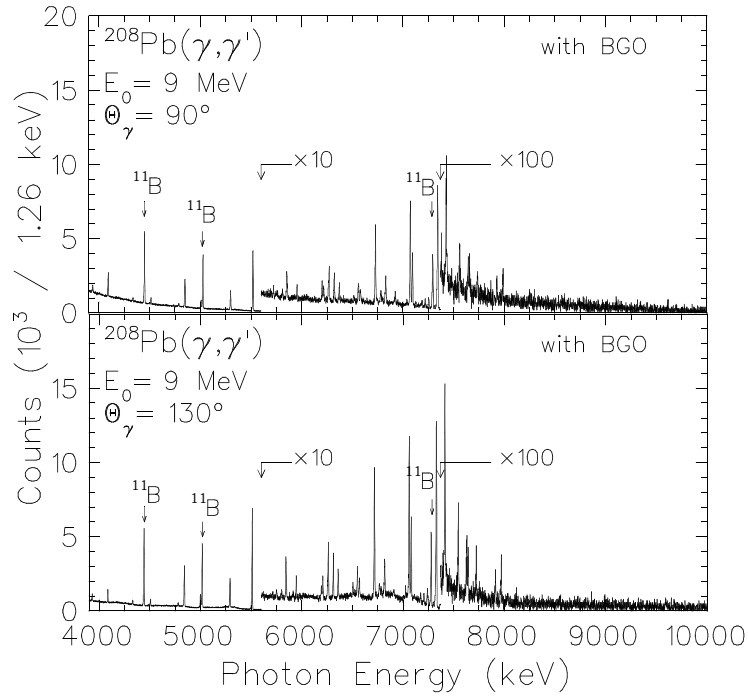


Fig. 12. Measured spectra at 90° and 130° around the neutron emission threshold.

Fig. 12 shows the energy-calibrated experimental (γ, γ') spectra of ^{208}Pb for the energy region between 6 and 9 MeV. The neutron separation energy of ^{208}Pb nucleus is 7368 keV, indicated by the arrow. Note that starting from this energy the counts are multiplied by a factor of 10 for a better visibility.

4.2 Assignment of the Transition Multipolarities

Using the ratio of peak intensities we can extract the multipolarities of the transitions. Fig. 13 shows these measured ratios at 90° and 130° . The predicted values for dipole and quadrupole scattering are 0.7 and 2.2. The errors are statistical only.

Besides well known E1 transitions strongly excited in the (γ, γ') reaction, one could also identify five quadrupole states, in particular the lowest 2^+ state at 4086 keV and one new 2^+ transition at 6912 keV.

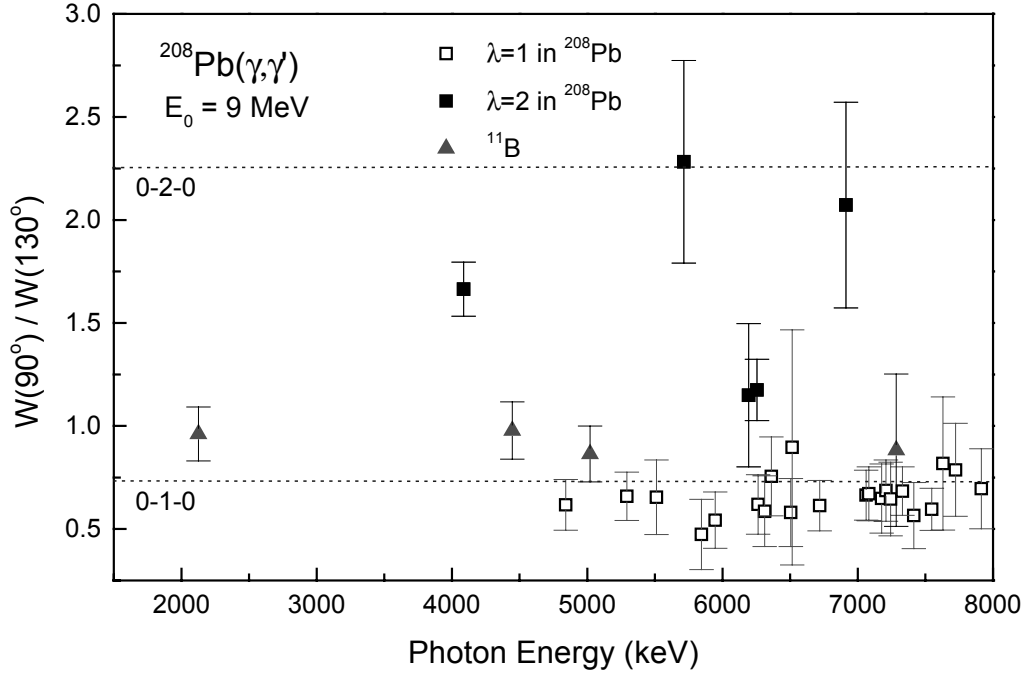


Fig. 13. Angular distributions of the transitions excited in the $^{208}\text{Pb}(\gamma,\gamma')$ reaction at $E_0=9$ MeV.

4.3 Further Data Analysis

From the peak areas the transition widths or lifetimes and the reduced transition strength can be derived. This is possible due to the absolute normalisation of the photon flux by measuring the well-known excitations in ^{11}B simultaneously using "sandwich" type targets. In this way the experimental problems of an absolute measurement of the photon flux $N_\gamma(E_x)$ from the bremsstrahlung source are avoided [28,29,30].

In this procedure we use the relationship between the integrated photon scattering cross section I_s and the properties of the involved nuclear levels. The measured peak area of a line in the NRF spectrum is proportional to the integrated cross section I_s (see Eq. 2.13) of the (γ,γ') reaction of the level in question via the relation

$$A_i = N_{\text{Target}} \cdot \int_{T_M} \Phi(E_x, E_0, t) dt \cdot \varepsilon(E_i) \cdot I_s^i \cdot W_{\text{eff}}^i(\theta) \cdot \frac{\Delta\Omega}{4\pi} . \quad (4.1)$$

Here N_{Target} is the total number of a target nuclei within the photon beam, T_M is the total time of the measurement, $\Phi(E_x, E_0, t)$ is the number of photons impinging the

unit of target surface per unit of time, $W_{eff}^i(\Theta)$ is the effective angle correlation function integrated over the solid angle $\Delta\Omega$ of the detector placed at the angle Θ , and E_x is the energy of the excited level.

The number of nuclei in a target is given by

$$N_{Target} = \rho \cdot \frac{N_A}{A} \cdot S, \quad (4.2)$$

where ρ is the surface density, S equals the area of the target surface, irradiated by the photon flux, N_A is Avogadro's number and A the mass number.

The yields of the reference transitions in the ^{11}B nucleus allow the determination of the product of the photon flux $N_\gamma(E_x)$ and the detector efficiency $\varepsilon(E_x)$ [31]. For $N_\gamma \varepsilon$ one obtains:

$$N_\gamma(E_x, E_0) \cdot \varepsilon(E_i) = \frac{A_i}{N_{Boron} \cdot I_s^i \cdot W_{eff}^i(\theta) \cdot \frac{\Delta\Omega}{4\pi}}, \quad (4.3)$$

where A_i is the peak area of the i -th Boron line. The integrated photon scattering cross section of the Boron lines used for the detection of $N_\gamma \varepsilon$ are listed in Table 1.

Table 1. Transitions in ^{11}B used for calibration.

| E_x [keV] | J^π | I_s^0 [10^3 eV fm^2] |
|----------------|---------|---------------------------------------|
| 2124.69 | $1/2^-$ | 5.1(4) |
| 4444.89 | $5/2^-$ | 16.3(6) |
| 5020.31 | $3/2^-$ | 21.9(8) |
| 7285.51 | $5/2^+$ | 9.4(7) |

The main source of systematic errors in this calibration procedure arises from the possibility of unidentified feeding of the reference levels by inelastic transitions from levels at higher energies. For ^{11}B the inelastic transitions are known. From the known branching ratios of the Boron transitions and the peak areas of the inelastic transitions the fractions of the peak areas due to inelastic transitions from higher lying states have been corrected.

In the case of ^{208}Pb the measured peak area A_i of a line and the integrated cross section are connected by the following relation:

$$A_i = N_{208Pb} \cdot N_\gamma(E_x, E_0) \cdot \varepsilon(E_i) \cdot I_s^i \cdot W_{eff}^i(\theta) \cdot \frac{\Delta\Omega}{4\pi} . \quad (4.4)$$

Then using the Eqs. 2.13, 2.16-2.18 one can extract the transition widths and the reduced transition probabilities $B(E1)\uparrow$, $B(E2)\uparrow$ and $B(M1)\uparrow$.

4.4 Obtained results

The experimental results for ^{208}Pb are summarised in Table 2. The excitation energy E_γ and the assigned spin J and parity π of each excited level are given. Furthermore the elastic transition strength Γ_0^2/Γ and the corresponding reduced transition probabilities $B(E1)\uparrow$, $B(E2)\uparrow$ or $B(M1)\uparrow$ are also listed. The excited level widths in the displayed Table, except for the transitions above the neutron threshold, are based on the assumption that the ground state branch is 100%.

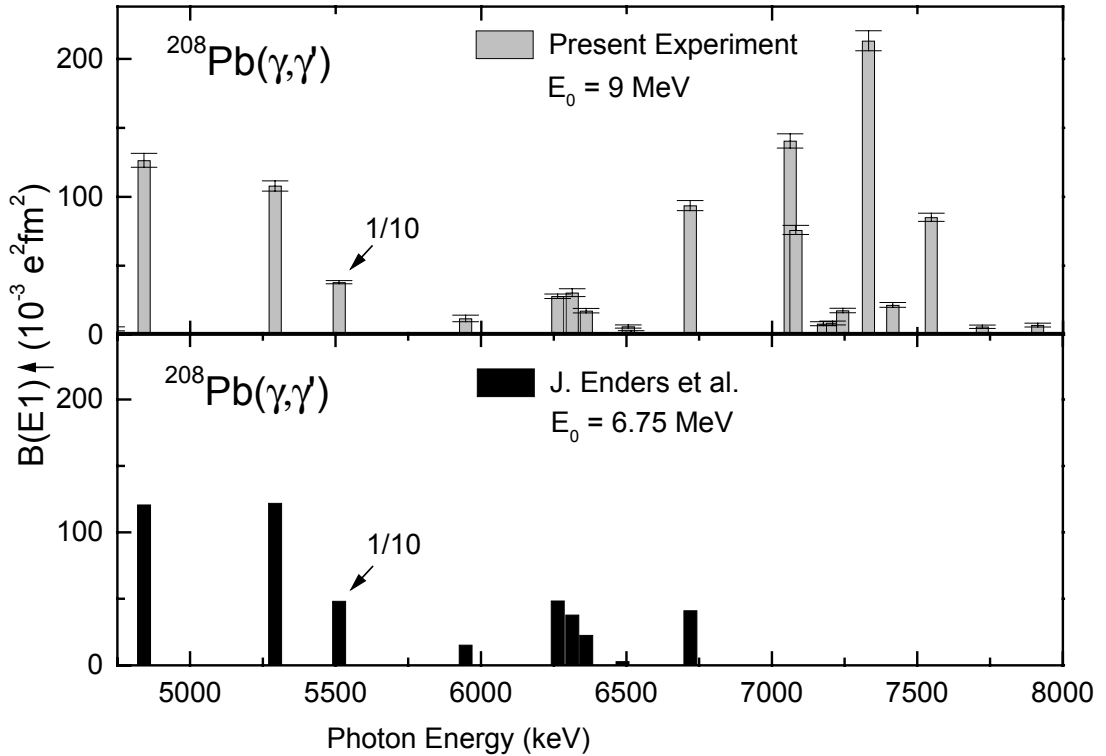


Fig. 14. Comparison of deduced $B(E1)\uparrow$ distribution in ^{208}Pb with the previous experiment [44].

Table 2. Experimental results of the $^{208}\text{Pb}(\gamma,\gamma')$ reaction at $E_0=9$ MeV.

| E_γ (keV) | J^π | Γ_0^2/Γ (eV) | $B(E1)\uparrow$ ($10^{-3} e^2\text{fm}^2$) | $B(E2)\uparrow$ ($e^2\text{fm}^4$) | $B(M1)\uparrow$ (μ^2_N) |
|------------------|---------|-----------------------------|---|---|----------------------------------|
| 4085.5 | 2^+ | 0.68(5) | | 3719(269) | |
| 4507.2 | 1 | 0.79(7) | 24.6(23) | | 2.22(21) |
| 4729.4 | 1 | 0.16(5) | 4.3(14) | | 0.39(13) |
| 4841.4 | 1^- | 5.01(20) | 126.5(50) | | |
| 5291.9 | 1^- | 5.58(19) | 107.9(37) | | |
| 5511.7 | 1^- | 22.24(68) | 381(12) | | |
| 5714.4 | 2^+ | 0.14(2) | | 141.6(230) | |
| 5844.5 | 1^+ | 1.50(16) | | | 1.95(21) |
| 5946.6 | 1^- | 0.86(18) | 11.8(24) | | |
| 6193.02 | 2^+ | 0.99(19) | | 40.7(23) | |
| 6255.1 | 2^+ | 1.06(10) | | 41.3(12) | |
| 6263.09 | 1^- | 2.39(14) | 27.9(16) | | |
| 6312.9 | 1^- | 2.67(25) | 30.4(29) | | |
| 6361.09 | 1^- | 1.56(15) | 17.4(16) | | |
| 6505.6 | 1 | 0.57(12) | 5.96(121) | | 0.54(11) |
| 6515.2 | 1 | 0.20(9) | 2.07(95) | | 0.19(9) |
| 6718.5 | 1^- | 9.91(38) | 93.7(36) | | |
| 6912.7 | 2^+ | 0.66(12) | | 259(47) | |
| 7062.1 | 1^- | 17.27(63) | 140.6(52) | | |
| 7081.9 | 1^- | 9.41(41) | 76.6(33) | | |
| 7176.3 | 1 | 1.02(19) | 7.9(15) | | 0.72(13) |
| 7208.0 | 1 | 1.11(18) | 8.5(13) | | 0.77(12) |
| 7242.8 | 1 | 2.32(21) | 17.5(16) | | |
| 7331.3 | 1^- | 29.32(101) | 213.2(73) | | |
| 7415.0 | 1 | 3.07(25) | 21.6(17) | | 1.95(16) |
| 7547.5 | 1^- | 1.57(20) | 85.2(13) | | |
| 7630.6 | 1^+ | 1.26(45) | | 0.92(26) | |
| 7722.6 | 1 | 0.93(19) | 5.8(12) | | 0.52(11) |
| 7913.0 | 1^- | 1.20(25) | 44.2(15) | | |

Table 3. Comparison of extracted transition widths with previous experiments.

| E_x (keV) | J^π | E_γ (keV) | Γ_0^2/Γ (eV) Present | Γ_0^2/Γ (eV) [13,44] | Γ_0^2/Γ (eV) [14] | Γ_0^2/Γ (eV) [15] | Γ_0^2/Γ (eV) [5] |
|----------------|---------|---------------------|-------------------------------------|-------------------------------------|----------------------------------|----------------------------------|---------------------------------|
| 4085.4 | 2^+ | 4085.5 | 0.68(5) | 0.45(3) | 0.68(15) | 0.51(20) | |
| 4842.1 | 1^- | 4841.4 | 5.01(20) | 4.78(31) | 5.0(8) | 6.3(22) | 6.9(14) |
| 5292.1 | 1^- | 5291.9 | 5.58(19) | 6.31(43) | 5.1(8) | 8.6(30) | 7.0(14) |
| 5512.0 | 1^- | 5511.7 | 22.24(68) | 28.3(21) | 22.3(34) | 28(10) | 21.4(22) |
| 5712 | 2^+ | 5714.4 | 0.14(2) | 0.13(2) | | | |
| 5846.1 | 1^+ | 5844.5 | 1.50(16) | 1.67(16) | | | 4.4(11) |
| 5946.4 | 1^- | 5946.6 | 0.86(18) | 1.13(11) | 1.0(3) | | |
| 6193 | 2^+ | 6193.02 | 0.99(19) | 0.57(7) | | | |
| 6255.6 | 2^+ | 6255.1 | 1.06(10) | 0.50(7) | | | |
| 6262 | 1^- | 6263.09 | 2.39(14) | 4.17(54) | 2.6(5) | 4.1(18) | 8.9(11) |
| 6312 | 1^- | 6312.9 | 2.67(25) | 3.34(52) | 3.2(6) | 1.0 | |
| 6363 | 1^- | 6361.09 | 1.56(15) | 2.05(37) | 1.6(4) | 0.5 | |
| | | 6505.6 | 0.57(12) | | | | |
| | | 6515.2 | 0.20(9) | | | | |
| 6720.5 | 1^- | 6718.5 | 9.91(38) | >4.37 | 7.6(15) | 15(6) | 13.0(16) |
| | | 6912.7 | 0.66(12) | | | | |
| 7063.5 | 1^- | 7062.1 | 17.27(63) | | 15.7(26) | 29(10) | |
| 7083.4 | 1^- | 7081.9 | 9.41(41) | | 8.8(15) | 14(5) | |
| | | 7176.3 | 1.02(19) | | | | |
| | | 7208.0 | 1.11(18) | | | | |
| 7240 | 1^- | 7242.8 | 2.32(21) | | 1.7(6) | | |
| 7332.5 | 1^- | 7331.3 | 29.32(101) | | 26.9(48) | 38(13) | 44.5(29) |
| | | 7415.0 | 3.07(25) | | | | |
| 7548.3 | 1^- | 7547.5 | 1.57(20) | | | | |
| 7631.9 | 1^+ | 7630.6 | 1.26(45) | | | | |
| | | 7722.6 | 0.93(19) | | | | |
| | | 7913.0 | 1.20(25) | | | | |

As can be seen from Fig. 14 and 15, the obtained results for E1 and E2 strength are in good agreement with the previous experiment on ^{208}Pb , which was carried out at the S-DALINAC [20].

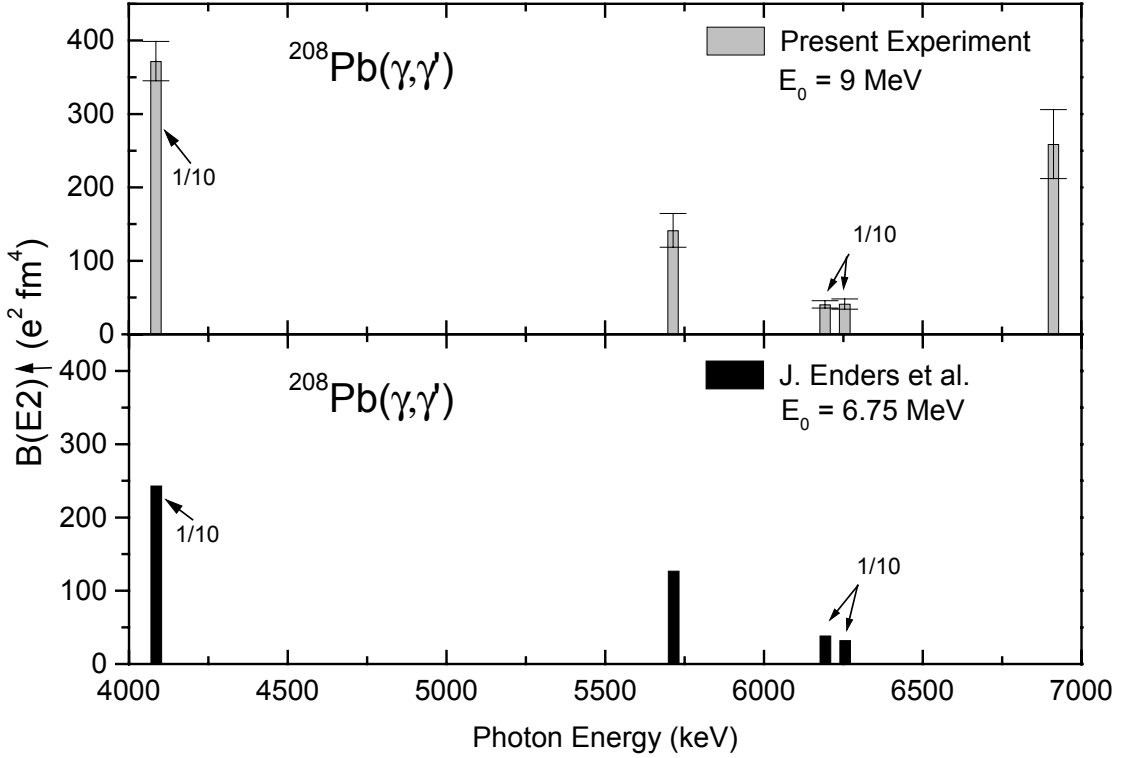


Fig. 15. Comparison of deduced $B(E2)\uparrow$ distribution in ^{208}Pb with the previous experiment [44]

A comparison with earlier experiments is shown in Table 3. The widths deduced from the present experiment agree roughly with those given in the literature [5,14,15].

The former experimental results by J. Enders et al. [13] were obtained with an end-point energy of 6.75 MeV. For the present experiment the possibility to determine transition widths at higher energies became possible.

At the energies above the separation energy of neutrons the total transition width is given by:

$$\Gamma = \Gamma_{\gamma} + \Gamma_n . \quad (4.5)$$

The problem of the investigation of transitions above the threshold by NRF results from the fact, that the neutron decay width Γ_n becomes dominating very fast in the total transition width Γ . Then, the integrated cross section measured in (γ, γ')

experiments, which is proportional to Γ_0^2/Γ , becomes extremely small. But surprisingly, several transitions were observed at energies up to more than 500 keV above the neutron threshold (see Table 4). This implies mean that either these transitions are extremely strong or the neutron decay width is very small because of peculiar structure features.

Table 4. Transitions above the threshold.

| Energy (keV) | J^π | $\Gamma_{\gamma 0}^2/\Gamma$ (eV) experimental | $\Gamma_{\gamma 0}$ (eV) | Γ_n (eV) |
|--------------|----------------|--|--------------------------|-----------------|
| 7415 | 1 | 3.06 | - | - |
| 7549 | 1 ⁻ | 1.6 | 12.7 | 92 |
| 7624 | 1 ⁻ | - | 21.3 | 3110 |
| 7633 | 1 ⁺ | 1.3 | 15.8 | 182 |
| 7722 | 1 | 0.9 | - | - |
| 7909 | 1 ⁻ | 1.2 | 7.6 | 40.5 |

As an example, we could not observe the 7624 keV level known from (n, γ) measurements [32] in the present experiment, because it has a neutron decay width much larger than the γ -decay width to the ground state Γ_0 . For the states at 7549 keV and 7631 keV Γ_0 was estimated using the known partial neutron decay widths from the literature [32]. The derived γ -decay width to the ground state was used to extract the reduced transition strength. For the transition to the level at 7909 keV the neutron decay width Γ_n was unknown up to now. Therefore in the present work this value was extracted from the experimental data, using Γ_0 from the literature.

Figure 16 displays the resulting electric dipole strength distribution in ^{208}Pb up to 8 MeV. The grey bars represent the strength obtained from the present experiment and the black bars reduced transitions probabilities from the literature [34], which were extracted from the $^{207}\text{Pb}(n,\gamma)$ reaction. These transitions could not be observed in the present (γ,γ') experiment because $\Gamma_n \gg \Gamma_\gamma$.

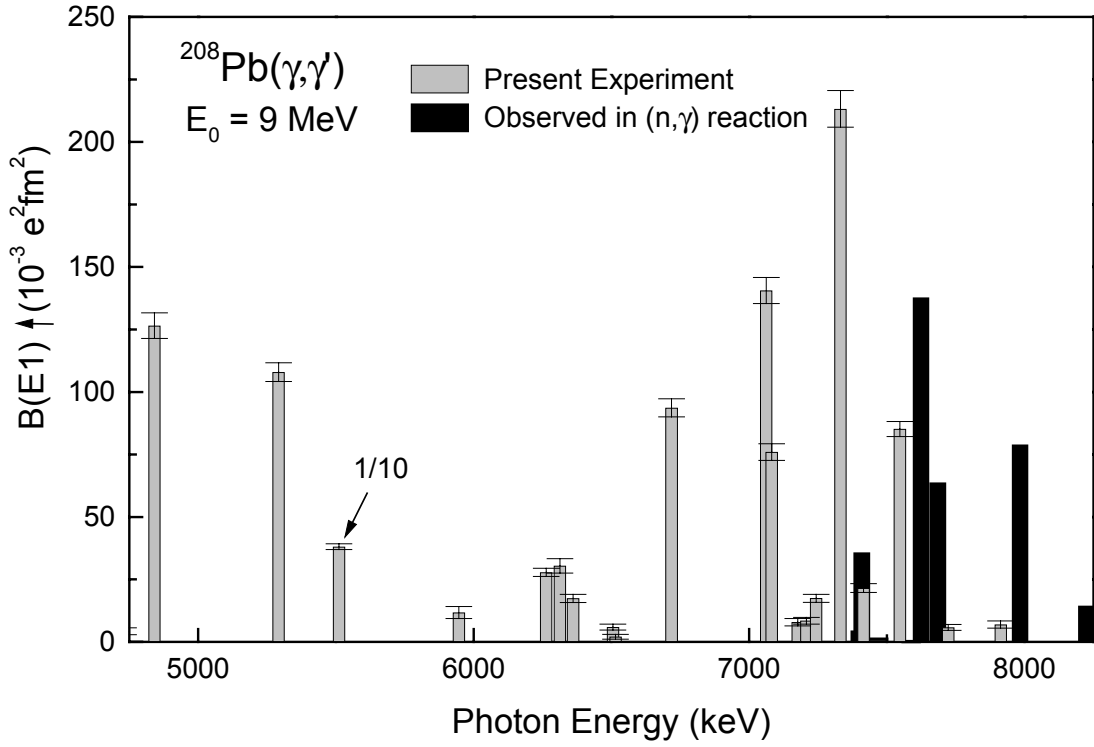


Fig. 16. Reduced dipole strength distribution.

From Fig. 17 it can be seen, that in the present (γ, γ') experiment only five E2 excitations were identified (grey bars). In the (n, γ) reaction, the observed γ -ray transitions are predominantly electric dipole or magnetic dipole transitions; electric quadrupole transitions at low energies are extremely rare. This has two reasons. First, the transition rates fall off rapidly with increasing multipole order. Second, if mixing with the giant resonances influences the (n, γ) reaction, the E2 transitions are weak for low-energy incident neutrons because the capturing state, which depends on the neutron separation energy S_n , is too far down on the tail of the giant quadrupole resonance. The best chance for observing E2 transitions from many neutron resonances occurs in a nucleus, which is heavy and has a large S_n value. The doubly magic nucleus ^{208}Pb is such a case and many E2 transitions to the ground state can be observed from (n, γ) reactions above the neutron threshold (black bars). The radiation widths were extracted from the literature [32].

Magnetic excitations were observed in the described experiment too. Figure 18 shows the extracted magnetic dipole strength distribution.

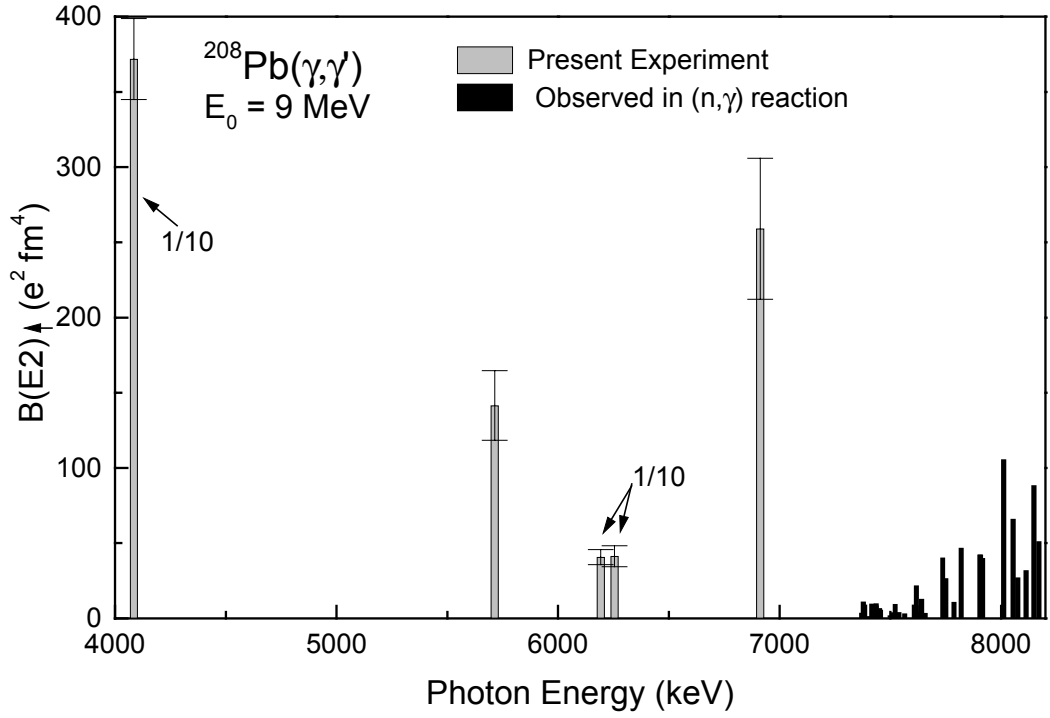


Fig. 17. $B(E2)_{\uparrow}$ ground state strength distribution for ^{208}Pb .

A large concentration of ground state M1 radiation strength has been detected in (n,γ) reactions [35], centred at an excitation energy of 7.9 MeV (black bars). This resonance contains one of the transitions, which was observed in the present $^{208}\text{Pb}(\gamma,\gamma')$ experiment (grey bars) at the energy of 7631 keV. The M1 resonance extends to higher energies and was observed in $(\vec{\gamma}, \vec{\gamma}')$ using tagged photons [33].

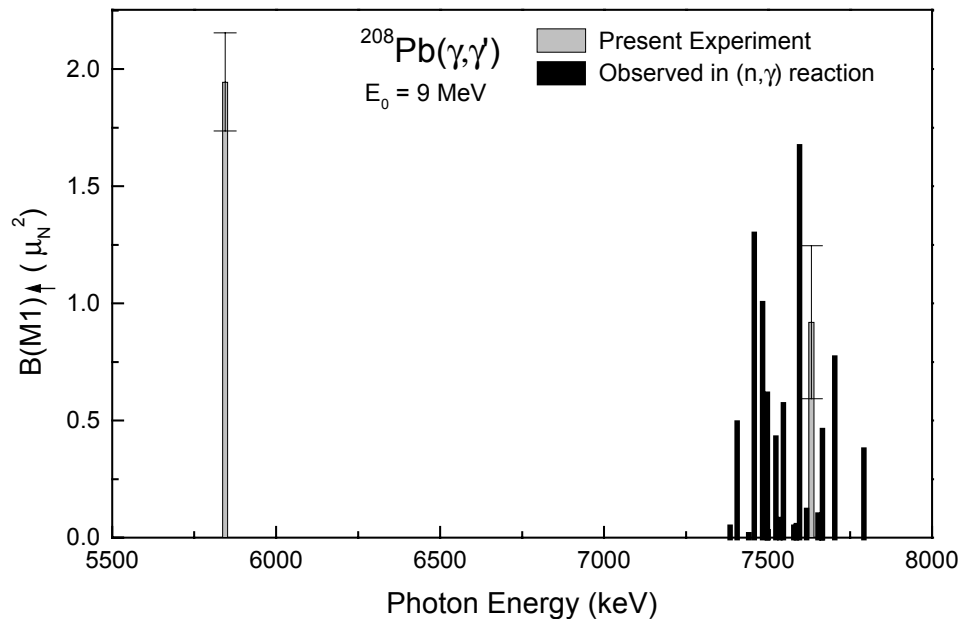


Fig. 18. $B(M1)_{\uparrow}$ strength distribution in ^{208}Pb .

4.5 Discussion

Nuclei with extreme neutron to proton ratio exhibit many interesting and unique structure phenomena: the weak binding of the outermost neutrons, pronounced effects of the coupling between bound states and the particle continuum, regions of nuclei with very diffuse neutron densities, the formation of neutron skin and halo structures. The multipole response of nuclei with large neutron excess has been the subject of many theoretical studies in recent years. In particular, studies of low-energy collective isovector modes provide important information on the isospin and density-dependent parts of the effective interactions used in nuclear structure models. The theoretical analysis has shown that the spectral distributions of neutron-rich nuclei are much more fragmented than those for well bound systems. This happens because protons and neutrons in the nuclei with the excess of neutrons feel very different effective potentials, and consequently display very different level spacings. In all calculations additional strength has been found below the normal giant resonance region. The low-energy collective isovector dipole mode, i.e. the Pygmy resonance, results from the excess neutrons oscillating out of phase with a core composed of equal number of protons and neutrons. A number of theoretical models have been applied in studies of the dynamics of Pygmy dipole resonances.

The phenomenon of low-lying isovector dipole strength was already studied almost thirty years ago in the framework of the **three-fluid hydrodynamic model**. By using a generalization of the Steinwedel-Jensen model to three fluids: the protons, the neutrons in the same orbitals as protons, and the excess neutrons, two normal modes of dipole vibrations were identified: vibrations of the protons against the two types of neutrons and the vibration of the excess neutrons against the proton-neutron core. In the case of neutron-rich nuclei, the latter mode corresponds to Pygmy resonances. For ^{208}Pb , in addition to the GDR state at 13.3 MeV, a low-lying Pygmy state at 4.4 MeV excitation energy was found in the analysis of Ref. [10]. The dipole strength of this state, however, was negligible (two orders of magnitude compared to the GDR state).

Results, based on the calculations in a **microscopic random phase approximation** [9], predict the existence around 9 MeV of a concentration of dipole excitations exhausting 2.4 % of the E1 sum rule. These states represent by their predominant neutron p-h character the analog of the halo excitation currently investigated in light nuclei.

One modification of this modern approach, the **relativistic mean-field theory**, is based on the following simple concepts: the nucleons are described as point particles, the theory is fully Lorenz invariant, the nucleons move independently in mean fields which originate from the nucleon-nucleon interaction. The interaction is mediated by the exchange of point-like effective mesons.

Using this model the low-lying E1 peaks were calculated in the energy region between 5 and 11 MeV [36]. Two prominent peaks were obtained: at 7.29 and 10.10 MeV (Fig.19). A detailed analysis shows, that the lower peak can be identified as the Pygmy dipole resonance. By analysing transition densities and velocity distributions, the authors have related the onset of Pygmy resonance at 7.29 MeV to the vibration of the excess neutrons against the inert core composed of protons and neutrons in the same shell model orbitals.

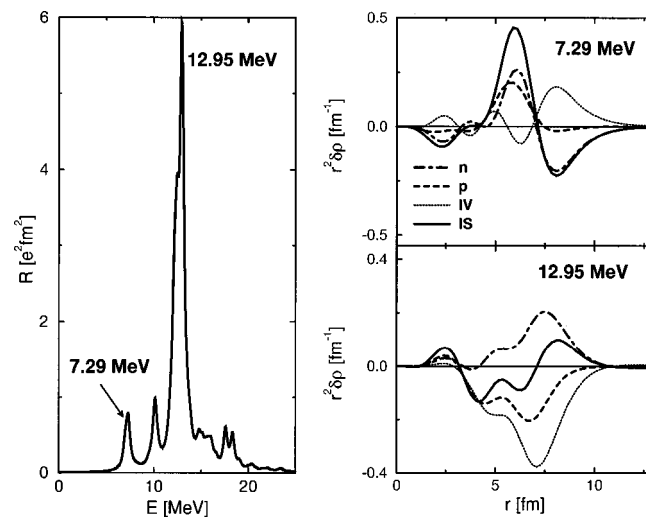


Fig. 19. Calculated with relativistic mean-field RPA isovector dipole strength distribution in ^{208}Pb (left panel), and transition densities for the two peaks at 7.29 and 12.95 MeV (right panel) [36]. Both isoscalar and isovector transition densities are displayed, as well as the separate proton and neutron contributions.

The authors point out at the lack of experimental data needed for the comparison with their calculations. Indeed, the experimental information on the fragmentation of E1 strength in ^{208}Pb was available only in the energy window 8–12 MeV, and below 6.5 MeV. In order to test the predictions of this relativistic random phase approximation analysis, it would be important to obtain experimental data also in the energy region between 6 and 8 MeV.

The present experimental data were obtained for the energy up to 9 MeV, so that they can make an important contribution in filling in this gap. Two regions of strong concentration of the dipole strength were observed: below 6.5 MeV and at 7.3 MeV. But a resonance clustering of E1 strength, which is observed between 4 and 6.5 MeV, cannot be attributed to an oscillation of the excess neutrons against the inert core [38]. The part of the total E1 strength, which is concentrated at 7.3 MeV, can be identified as a Pygmy dipole resonance from the comparison with relativistic mean-field RPA calculations.

5. Conclusion

By means of resonant scattering of real photons a highly sensitive study of the dipole strength distribution in the even-even ^{208}Pb nucleus has been performed at the S-DALINAC covering the excitation energy range of up to 9 MeV. The experiment aimed to search for the Pygmy dipole resonance, being predicted by different models at different energies. These models includes: the three-fluid hydrodynamic model [10], density functional theory [7], and the Hartree - Fock plus random phase approximation (RPA) with Skyrme forces [9].

A detailed picture of the fine structure of the dipole strength near and above the neutron emission threshold in ^{208}Pb has been obtained. About 12 dipole transitions were observed, in particular several transitions were found above the neutron emission threshold. The excitation energies and the ground state transitions widths of the corresponding levels have been determined. The strong fragmentation of the dipole strength was observed. The main E1 strength, observed in this experiment, was concentrated in two energy regions near 5.5 and 7.3 MeV. The last one can be argued as a possible candidate for Pygmy dipole resonance [36].

6. References

- [1] M. N. Harakeh and A. van der Woude, Giant resonances: fundamental high-frequency modes of nuclear excitation. (N. Y.: Oxford University Press, Oxford, 2001)
- [2] B. L. Berman and S. C. Fultz, *Rev. Mod. Phys.* 47, 713-761 (1975)
- [3] A. Richter, *Nucl. Phys. A553* (1993) 417c
- [4] R.-D. Herzberg, J. Enders, P. von Brentano, J. Eberth, A. Fitzler, C. Fransen, H. Kaiser, L. Käubler, P. von Neumann-Cosel, N. Pietralla, V. Yu. Ponomarev, H. Prade, A. Richter, H. Schnare, R. Schwengner, S. Scoda, H. G. Thomas, H. Tiesler, D. Weisshaar, I. Wiedenhöver, *Phys. Rev. C60* (1999) 051307-1
- [5] R. M. Laszewski and P. Axel, *Phys. Rev. C19* (1979) 342
- [6] P. van Isacker, M. A. Nagarajan, and D. D. Warner, *Phys. Rev. C45* (1992) R13
- [7] J. Chambers, E. Zaremba, J. P. Adams and B. Castel, *Phys. Rev. C50* (1994) R2671
- [8] P. Mohr, T. Hartmann, K. Vogt, S. Volz, and A. Zilges, Proceedings of the International Nuclear Physics Conference INPC 2001, Berkeley, Ca, USA, July 29 - August 03, 2001, in press.
- [9] J. P. Adams, B. Castel and H. Sagawa, *Phys. Rev. C53* (1996) 1016
- [10] R. Mohan, M. Danos and L. C. Biedenharn, *Phys. Rev. C3* (1971) 1740
- [11] J. Enders, P. von Brentano, J. Eberth, A. Fitzler, C. Fransen, R.-D. Herzberg, H. Kaiser, L. Käubler, P. von Neumann-Cosel, N. Pietralla, V. Yu. Ponomarev, A. Richter, H. Schnare, R. Schwengner, S. Skoda, H. G. Thomas, H. Tiesler, D. Weisshaar, I. Wiedenhöver, *Nucl. Phys. A674* (2000)

- [12] T. Hartmann, J. Enders, P. Mohr, K. Vogt, and A. Zilges, Phys. Rev. Lett. 85 (2000) 274
- [13] J. Enders, Dissertation, TU-Darmstadt (1999)
- [14] T. Chapuran, R. Vodhanel and M. K. Brussel, Phys. Rev. C22 (1980) 1420
- [15] D. F. Coope, L. E. Cannell and M. K. Brussel, Phys. Rev. C15 (1977) 1977
- [16] F. R. Metzger, Phys. Rev. C18 (1978) 1603
- [17] F. R. Metzger, Phys. Rev. C17 (1978) 939
- [18] H. A. Bethe and G. Placzek, Phys. Rev. 51 (1937) 450
- [19] U. Kneissl, H. H. Pitz and A. Zilges, Prog. Part. Nucl. Phys. 37 (1996)
- [20] A. Richter, Proceedings of the Fifth European Particle Accelerator Conference, ed. S. Meyers et al., (IOP Publishing, Bristol, 1996) 110
- [21] P. Mohr, J. Enders, T. Hartmann, H. Kaiser, D. Schiesser, S. Schmitt, S. Volz, F. Wissel and A. Zilges, Nucl. Instr. Meth. A423 (1999) 480
- [22] D.A. Fraser, The Physics of Semiconductor Devices, 4th Ed. (Oxford University Press, Oxford, 1986)
- [23] G.F. Knoll, Radiation Detection and Measurement, 2nd Ed. (Wiley, New York, 1989)
- [24] B. Schlitt et al., Nucl. Instr. Meth. A337 (1994) 416
- [25] J. Ebers, H. G. Thomas, D. Weisshaar, F. Becker, B. Fiedler, S. Scoda, P. von Brentano, C. Gund, L. Palafox, P. Reiter, D. Schwalm, D. Habs, T. Servene, R. Schwengner, H. Schnare, W. Schulze, H. Prade, G. Winter, A. Jungclaus, C. Lingk, C. Teich, K. P. Leib, Prog. Part. Phys. 38 (1997) 29
- [26] L. M. Garcia-Raffi, J. L. Tain, J. Bea, A. Gadea, L. Palafox, J. Rico, B. Rubio, Nucl. Instr. Meth. A381 (1996) 462
- [27] A. Keenan, Ph. D. Thesis, University of Liverpool (1999)
- [28] K. Govaert, F. Bauwens, J. Bryssinck, D. De Frenne, E. Jacobs and W. Mondelaers, Phys. Rev. C57 (1998) 2229

- [29] T. Hartmann, Diplomarbeit, TU-Darmstadt (1999)
- [30] S. Volz, Diplomarbeit, TU-Darmstadt (2001)
- [31] R. Moreh, W. C. Sellyey and R. Vodhanel, Phys. Rev. C22 (1980) 1820
- [32] M. J. Martin, Nuclear Data Sheets 47 (1986) 797; Evaluated Experimental Nuclear Structure Data File, National Nuclear Data Center, Brookhaven/NY (1999)
- [33] R. M. Laszewski, R. Alarcon, D. S. Dale, and S. D. Hoblit Phys. Rev. Lett. **61** (1988) 1710
- [34] R. J. Holt, H. E. Jackson, R. M. Laszewski and J. R. Specht, Phys. Rev. C20 (1979) 93
- [35] S. Raman, M. Mizumoto and R. L. Macklin, Phys. Rev. Lett. 39 (1977) 598
- [36] D. Vretenar, N. Paar, P. Ring and G. A. Lalazissis, Phys. Rev. C63 (2001) 047301
- [37] S. Ramchandran and J. McIntyre, Phys. Rev. 179 (1969) 1153
- [38] J. Enders, P. von Brentano, J. Eberth, A. Fitzler, C. Fransen, R.-D. Herzberg, H. Kaiser, L. Käubler, P. von Neumann-Cosel, N. Pietralla, V. Yu. Ponomarev, H. Prade, A. Richter, H. Schnare, R. Schwengner, S. Scoda, H. G. Thomas, H. Tiesler, D. Weisshaar, I. Wiedenhöver, Phys. Lett. B486 (2000) 279
- [39] J. Reif et al., Nuclear Physics A 620 (1997) 1
- [40] J. Enders, P. von Brentano, J. Eberth, R.-D. Herzberg, N. Huxel, H. Lenske, P. von Neumann-Cosel, N. Nicolay, N. Pietralla, H. Prade, J. Reif, A. Richter, C. Schlegel, R. Schwengner, S. Skoda, H. G. Thomas, I. Wiedenhöver, G. Winter, A. Zilges, Nuclear Physics A 636 (1998) 139
- [41] W. Biesiot, Ph. B. Smith, Phys. Rev. C24 (1981) 808

- [42] K. Wienhard, K. ackermann, K. Bangert, U. E. P. Berg, C. Bläsing, W. Naatz, A. ruckelshausen, D. Rück, R. K. M. Schneider, and R. Stock, Phys. Rev. Let. 49 (1982) 18
- [43] V. Yu. Ponomarev, Nucl. Phys. A 635 (1998) 470
- [44] J. Enders, P. von Neumann-Cosel, V. Yu. Ponomarev and A. Richter, Nuclear Phys. A 612 (1997) 239
- [45] C. D. Bowman, B. L. Berman and H. E. Jeckson, Phys. Rev. 178 (1969) 1827
- [46] D. J. Horen, J. A. Harvey, and N. W. Hill, Phys. Rev. Let. 38 (1977) 1344
- [47] C. D. Bowman, R. J. Baglan, B. L. Berman, and T. W. Phillips, Phys. Rev. Let. 25 (1970) 1302
- [48] D. J. Horen, J. A. Harvey, and N. W. Hill, Phys. Rev. C18 (1978) 722

Acknowledgements

At this place I would like to thank all the persons who have contributed to the success of this work.

On the first place I would like to sincerely thank Professor Dr. Dr. h.c. mult. Achim Richter for the given great opportunity to work on such an exciting topic under Your supervision, and for the possibility to take part in Joint Universities Accelerator School 2002. I am sure that this will motivate me even more in my future scientific work.

Further on I would like to thank Dr. Peter von Neumann-Cosel for numerous valuable physical discussions during the realisation of this diploma project.

I address my heartfelt gratitude to Dr. Harald Genz for Your every day help, care and support.

Without priceless help of Dipl. Phys. Artem Shevchenko this work would not be imaginable.

I would like to express my gratitude to Dipl.-Phys. Stephan Volz Dipl.-Phys. Timo Hartmann, Dipl.-Phys. Frank. Hofmann, Dipl.-Phys. Yaroslav Kalmykov, Dipl.-Phys. Karsten Vogt for numerous advises, the significance of which it is difficult to overestimate.

I am grateful to Dr. E. Shmatko, Dr. A. Schus and Chair of the Experimental Nuclear Physics of the Karazin National University Kharkiv (Ukraine) for the time they have spent for my education.

Finally, my heartfelt gratitude to my family - my parents Ganna and Valery and my brother Dipl. Phys. Aleksandr Ryezayev. Your thoughts and your care were supporting me very much during my study in the Karazin Kharkiv National University and during my staying in Darmstadt.